https://doi.org/10.1016/j.jece.2020.105022

Non-oxidative decomposition of propane: Ni-Cu/Al_2O_3 catalyst for the production of CO_2-free hydrogen and high-value carbon nanofibers

D. Torres*, J.L. Pinilla, I. Suelves

Instituto de Carboquímica, CSIC. C/ Miguel Luesma Castán, 4. 50018. Zaragoza, Spain

Abstract

A Ni-Cu/Al_2O_3 catalyst was tested in the thermal decomposition of propane to produce CO_2-free hydrogen and high value-added carbon nanofibers (CNF), the quantity and quality of which are key to making the process economically viable. The effect of temperatures in the range 550-750 ºC and space velocities from 24 to 240 l g_{Cat}^{-1} h^{-1} on the product distribution, conversion, H_2 selectivity and carbon formation rate (CFR) was evaluated. In addition to H_2, CH_4 and C_2H_4 together with small amounts of C_2H_6 were detected in the reaction gases. While propane conversion overpassed 90 % at 700 ºC and higher temperatures, H_2 selectivity reached 40 % for low space velocities (24 l $g_{Cat}^{-1}h^{-1}$). Likewise, the CFR increased with temperature to 50 g_C g_{Cat}^{-1} h^{-1} at 700 ºC, doubling the rates reported for methane or ethane as the feedstock and same reaction conditions. The CNF, thoroughly characterized by XRD, N_2 physisorption, SEM and TEM, exhibited bimodal and wide diameter distribution (6-120 nm) and fishbone morphology with high graphitic order (interplanar distance: 0.339-0.347 nm, and crystal sizes around 5 nm) and good textural properties (specific surface area: 100-190 m^2 g^{-1} and total pore volume: 0.23-0.45 cm^3 g^{-1}).

* Corresponding author. E-mail address: dtorres@icb.csic.es (D. Torres).

Keywords: *Ni-Cu bimetallic catalyst; hydrogen production; catalytic decomposition of propane; fishbone carbon nanofibers.*

1. INTRODUCTION

The hydrogen production industry worldwide tends to redirect the currently established technologies towards processes with free-CO_2 emissions either by capturing and storing technologies or by preventing its formation. With this objective, the decomposition of methane and higher hydrocarbons for the concurrent production of hydrogen and high-value carbon nanofilaments has been intensively studied [1, 2]. The decomposition reaction of higher hydrocarbons (see Equation 1) is more complex than that of methane since the reaction takes place through a stepwise process which includes the C–C bonds cleavage and the formation of methane or another intermediate hydrocarbon (alkane or alkene) before the definitive formation of H_2 and carbon nanofilaments [3]. However, thermal decomposition of butane or propane is easier than that of methane due to the relatively lower C–H bond energies: 381 and 406 kJ/mol, respectively, compared to that in methane (439 kJ/mol) [4]. In this way, since C–C bond energy is lower than that of C–H, the reaction of higher hydrocarbons would start via its homogeneous decomposition by a free radical reaction mechanism [5, 6].

$$C_nH_{2n+2} \rightarrow nC + (n+1)H_2 \qquad \textbf{Equation 1}$$

In addition to offering greater ease in separating H_2 from the initial molecule than methane, propane also is a low cost and high available fuel which makes it a direct alternative to produce free-CO_x H_2. Non-catalytic thermal decomposition of propane generates mainly H_2, CH_4 and C_2H_4, and small quantities of C_2H_6 and C_3H_6 during reaction [3, 6, 7]. Solovyev *et al.* investigated both the non-catalytic and the catalytic thermal decomposition of propane [6].

Massive Ni/Al_2O_3, $Ni-Cu/Al_2O_3$ and $Ni-Cu/SiO_2$ catalysts were tested in the range of 500-700 ºC for the production of hydrogen and platelet and stacked-cone carbon nanofibers. The non-catalytic process began at 525 ºC being H_2, CH_4, C_2H_6 and C_2H_4 the main reaction gas products. At 700 ºC the propane conversion was around 90 % but only 11 and 40 vol. % of H_2 and CH_4 were produced, respectively. CH_4 is produced more extensively than H_2 due to, as before mentioned, the breaking of the C–C bond is more favoured than that of the C–H bond [6].

Theoretically, catalytic decomposition can be applied to hydrocarbons in the range C1-C10 [8]. Otsuka *et al.* [9, 10] reported that cracking of high molecular weight alkanes and alkenes on a Ni/SiO_2 catalyst produces methane and hydrogen as products along with small amounts of other high molecular weight hydrocarbons. Likewise, carbon was deposited in the form of carbon nanofibers (CNF). According to several authors, the catalytic dehydrogenation of propane can occur as shown in Equation 2 [6, 10, 11]. Hydrocarbons decompose into hydrogen and carbon, while methane is produced by carbon hydrogenation.

$$C_3H_8 \rightarrow C_2H_5 + CH_3 \rightarrow 3C + 4H_2 \rightarrow 2C + CH_4 + 2H_2 \qquad \textbf{Equation 2}$$

Although carbon black or activated carbon exhibited interesting performances as catalysts for H_2 production by thermal propane decomposition [12, 13], both high H_2 selectivity or the formation of high-quality carbon nanofilaments would require specific active phases in the catalyst like Ni, Co, Mo, Pd or Fe [3, 6, 7, 14-17]. Catalysts using Ni as the main active phase or as an element dopant, widely used for hydrogenation reactions, showed high activity for obtaining H_2 and carbon nanofilaments (nanotubes and nanofibers) by thermal propane decomposition [3, 6, 7, 14, 16-19]. As has already been widely verified in the catalytic decomposition of methane [20-25], Cu as a dopant improved the activity of Ni-based catalysts also resulting in longer life-times and higher H_2 and carbon formations. However, this

behaviour of Ni-Cu catalysts in the decomposition of propane has only been reported in a very few works [6, 16], in which the textural and structural properties of the carbon nanofilaments obtained are not determined. Solovyev *et al.* reported an H_2 concentration of 38 vol.% at 550 ºC for Ni catalysts, while Ni-Cu catalysts could overpass the 80 vol. % at 700 ºC [6]. In the same study, Ni-Cu catalysts exhibited the highest carbon formations and H_2 yields at temperatures of about 650 or 700 ºC depending on the Ni/Cu ratio presented in the catalyst. Neuberg *et al.* tested Ni/Al_2O_3, catalysts for propane decomposition in a higher temperature range: 700-1100 ºC obtaining in all cases a full propane conversion [14]. Likewise, C_3H_6, C_2H_4 or C_2H_6 were undetected in the gas stream. H_2 yields close to 100 % were obtained for temperatures higher than 900 ºC. On the other hand, the addition of an element dopant like Co or Fe ($Ni\text{-}Co/Al_2O_3$ and $Ni\text{-}Fe/Al_2O_3$ catalysts) resulted in higher formations of CH_4 than the undoped catalysts.

In this work, the performance of a $Ni\text{-}Cu/Al_2O_3$ catalyst (78:06:16, mol. %), used in our previous studies on non-oxidative thermal decomposition of methane [26, 27] and ethane [28], was investigated in the catalytic decomposition of propane to produce hydrogen and CNF. The importance of this study lies in demonstrating that this catalyst promoted the formation of large amounts of high value-added CNF by a potentially industrial process to produce H_2 without the formation of CO_2 as a by-product. The nanocarbon obtained is key to economizing the process, so its quantity and quality are of great importance. This catalyst, besides showing a wide versatility in the catalytic decomposition of methane or ethane, exhibited in this work one of the highest formations of carbon nanofilaments found in the literature by propane decomposition. Additionally, a detailed study of the effect of the reaction temperature (from 550 to 750 ºC) and the weight hourly space velocity (WHSV; from 24 to 120 l g_{Cat}^{-1} h^{-1}) on the propane conversion, hydrogen selectivity and carbon formation rate was carried out. On the other hand, the as-obtained carbon nanofibers showed interesting structural, textural and

morphological characteristics according to a thorough characterization performed by XRD, N_2 physisorption, SEM and TEM.

2. MATERIALS AND METHODS

2.1. Catalyst preparation

Ni-Cu/Al_2O_3 (78:06:16; molar %) catalyst was prepared from the respective salts ($Ni(NO_3)_2$, $Cu(NO_3)_2$ and $Al(NO_3)_3$) by the fusing method [20, 26, 29]. Nitrates of Ni, Cu and Al were mixed in the desired composition and calcined at 350 ºC for 1 h and 450 ºC for 8 h. The preparation and detailed physicochemical characterization (XRD, TPR, N_2 physisorption, SEM-EDX and ICP-OES) of this catalyst, both fresh and reduced, can be found in the works previously mentioned [20, 26, 28, 29]. The fresh catalyst (specific surface area = 80 m^2 g^{-1}), composed of 23 nm Cu-doped NiO nanoparticles (according to XRD), resulted in a catalyst with Ni-Cu alloy nanoparticles of 28 nm on average after reduction stage. These Ni-Cu alloy nanoparticles are integrated with Al_2O_3 that acts merely as a textural promoter. Due to the presence of Cu and the low calcination temperature used in the synthesis of the fresh catalyst, the formation of spinels, observed in similar catalysts [30], did not take place.

2.2. Propane decomposition tests

The catalytic decomposition of propane was carried out in a fixed-bed quartz reactor (60 cm height and 1.8 cm i.d.) at atmospheric pressure. Before the activity tests, 50 mg of fresh Ni-Cu-Al_2O_3 catalyst was subjected to reduction with H_2 (50 ml min^{-1}) at 550 ºC and 1 h. Subsequently, the temperature was raised using a N_2 flow to the desired operating temperature. Once the temperature was reached, pure propane (99.99 %) was fed into the reactor for propane decomposition at the desired weight hourly space velocity (WHSV, defined as the propane flow rate per gram of fresh catalyst) for up to a maximum of 120 min. The time on stream (TOS) tests were performed isothermally at different temperatures (in the range of 550-750 ºC) and a

constant WHSV of 120 l g_{Cat}^{-1} h^{-1}. Additionally, TOS tests varying the WHSV in a range from 24 to 240 l g_{Cat}^{-1} h^{-1} and 700 ºC were also carried out.

Exit gases were sampling using bags and analysed by gas chromatography coupled to TCD (micro GC Varian CP4900 and Varian 3400 chromatographs). Propane conversion and selectivity to H_2 were calculated as follows:

$$C_3H_8 \text{ conversion (\%)} = (\text{moles of } C_3H_8 \text{ reacted/moles of } C_3H_8 \text{ fed}) \times 100 \qquad \textbf{Equation 3}$$

$$H_2 \text{ selectivity (\%)} = (\text{moles of } H_2 \text{ formed/total moles of products}) \times 100 \qquad \textbf{Equation 4}$$

Where the *total moles of products* include all gases, including H_2, as well as the solid carbon formed.

The carbon formation rate (CFR) was determined by applying the carbon mass balance between the propane fed and the un-reacted one and other hydrocarbons formed, as determined by GC, for full reaction time (maximum 120 min).

2.3. Characterization techniques

Powder X-ray diffraction (XRD) analysis of carbon products was performed with a PANalytical diffractometer using a configuration of θ/2θ, Ni-filtered CuKα radiation and a secondary graphite monochromator. The angle range scanned was 10-100º using 0.028º counting step and 20 s counting time. Diffractograms were processed using X'Pert Highscore Plus software to obtain refined structural parameters of the phases by the Rietveld method. The average domain size, L_c, of the deposited carbon was calculated from the width of the graphite (002) plane reflection by applying Scherrer's equation.

The textural properties were measured by N_2 physisorption at 77 K in a Micrometrics ASAP2020 apparatus. The specific surface areas (S_{BET}) and total pore volumes (V_t) were calculated by applying the BET method to the respective N_2 adsorption isotherms and from the

adsorbed volume of N_2 at p/p_0= 0.97, respectively. Besides, the micropore surface area (S_{mic}) was calculated by the Dubinin–Radushkevich equation.

The morphological appearance of carbon nanomaterials was studied with a scanning electron microscope (SEM) (Hitachi S-3400), and a transmission electron microscopy (TEM) (JEOL 2010). TEM was performed with a field emission electron source working in image mode at 200 kV.

3. RESULTS

3.1 Parametric study of the operating conditions

Initially, the catalytic decomposition of propane was studied by varying both the operating temperature and the WHSV. Figure 1a shows the variation of the composition of the product gases after 10 min of reaction (initial performance) as a function of the operating temperature. Hydrogen and ethylene (C_2H_4) increased as the temperature did and the propane was consumed. On the other hand, the methane concentration fluctuates with temperature yielding maximums and minimums in the range of 38-40 and 29-32 %, respectively. Finally, ethane concentration reaches values lower than 1 %, regardless of the operating temperature. As a result of these variations, both propane conversion and selectivity to H_2 increased with temperature as shown in Figure 1b. However, the increase of the later was only 11 %, from 26 % (550 ºC) to 37 % (750 ºC). Likewise, initial propane conversion was almost complete using 750 ºC (98 %). The C2 products (mainly C_2H_4) could be formed by the non-catalytic decomposition of propane, in parallel to the catalytic one, due to the effects of loss of catalyst activity [3, 6]. Considering the CFR (determined from the carbon yield of the catalyst for the complete reaction at different temperatures), this increased with temperature until reach a maximum of 50 $g_C\ g_{Cat}^{-1}\ h^{-1}$ for 700 ºC. The temperature at which the maximum CFR is obtained (700 ºC) coincides with that observed for methane (19 $g_C\ g_{Cat}^{-1}\ h^{-1}$) [27] catalytic decomposition using this same catalyst. In

the case of the ethane catalytic decomposition, the maximum CFR was obtained in the range 650-700 ºC (23 and 22 $g_C\ g_{Cat}^{-1}\ h^{-1}$, respectively) [28]. As expected considering the increasing molar carbon contribution in these hydrocarbons: CH_4 (C/H = 0.250) < C_2H_6 (0.333) < C_3H_8 (0.375), propane obtained the highest formation of nanostructured carbon per mol. On the other hand, an abrupt decrease in CFR was obtained at 750 ºC coinciding with the increase in ethylene concentration (see Figure 1a). The formation of the latter could be achieved through a competitive and non-catalytic reaction with respect to the formation of carbon. In fact, it is observed how the local maximum of ethylene concentration obtained at 650 ºC (Figure 1a) coincides with a local minimum of CFR for the same temperature (Figure 1b).

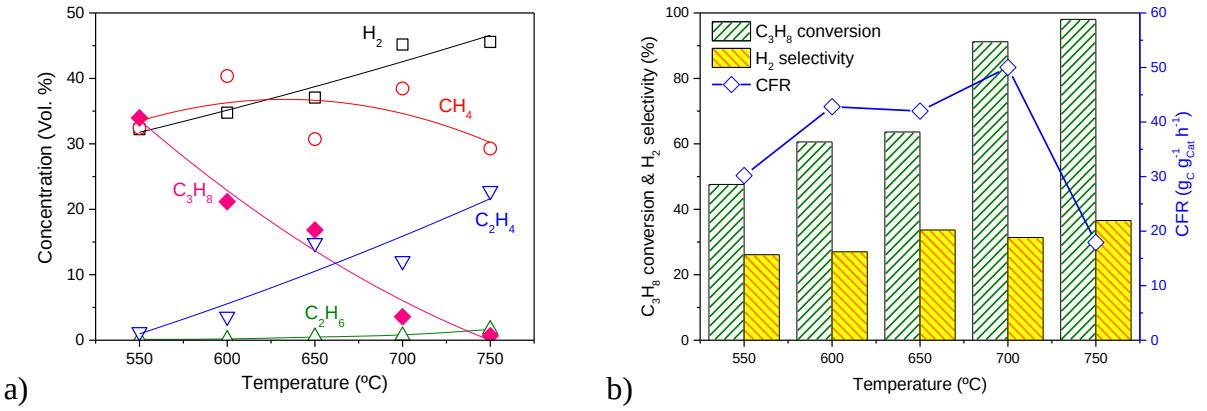

Figure 1 Influence of temperature on the catalytic decomposition of propane: a) initial product gas composition; b) propane conversions and H_2 selectivities after 10 min of reaction, and CFR values for the complete reaction. WHSV = 120 l $g_{Cat}^{-1}\ h^{-1}$.

The distribution of the reaction products in standard propane decomposition experiments carried out at 550 and 750 ºC (minimum and maximum operating temperatures studied in the present work), and using a WHSV of 120 l $g_{Cat}^{-1}\ h^{-1}$ is shown in Figure 2. The composition of the exit gases was a mixture of hydrogen, methane, ethane and ethylene, together with unreacted propane. As before commented, the propane conversion increased with temperature so the

almost absence of unreacted propane in the exit gases at 750 ºC was expected. At 550 ºC, the propane conversion decays rapidly with time. On the other hand, although H_2 formation was constant (28-33 %) during the experiment at this temperature, CH_4 formation decreased as fast as the unreacted propane concentration increased. This indicates that the decomposition of propane at this temperature mainly occurs by a dehydration pathway towards CH_4 formation as expressed in Equation 2 [6, 10, 11]. At 750 ºC, H_2, CH_4 and C_2H_4 were the main gases obtained during the reaction. However, while H_2 formation was decreased as the test proceeded (from 46 to 19 %), that of CH_4 and C_2H_4 increased from 29 and 23 to 35 and 43 %, respectively. In this case, C_2H_4 could be formed via a parallel non-catalytic reaction [6]. The thermal process is more accentuated at this temperature so the CH_4 formation increases being the C-C bond scission more favoured in the overall reaction.

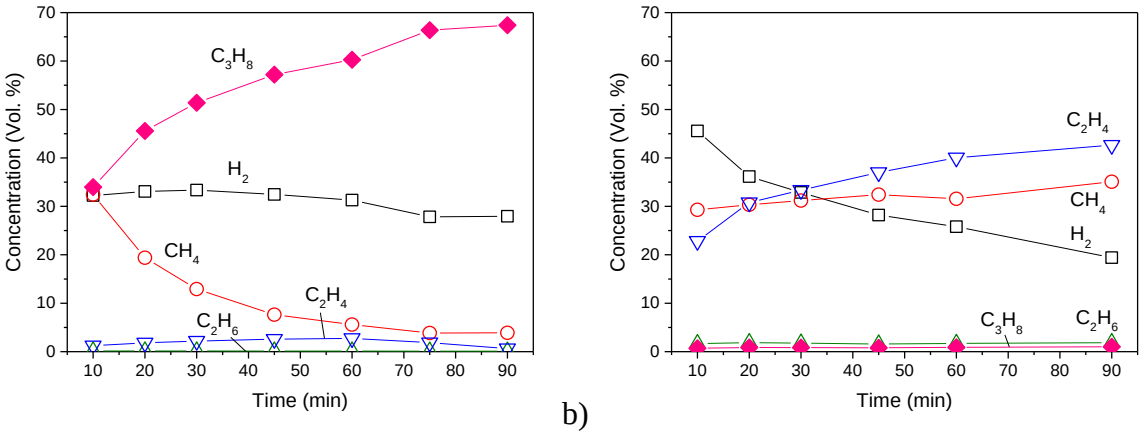

Figure 2 Distribution of products of the catalytic decomposition of propane at a) 550 ºC; and b) 750 ºC. WHSV = 120 l g_{Cat}^{-1} h^{-1}.

Considering the influence of WHSV on the catalytic decomposition of propane, experiments at 700 ºC varying the WHSV from 24 to 240 l g_{Cat}^{-1} h^{-1}were performed as shown in Figure 3. The H_2 selectivities decreased from 40 to 30 % as the WHSV increased from 24 to 60 l g_{Cat}^{-1} h^{-1}, while propane conversion remained at 99 %. However, higher WHSV like 120 or 240 l g_{Cat}^{-1} h^{-}

^{1} resulted in C_3H_8 conversions of 91 and 86 %, respectively, and H_2 selectivities of 31 and 35 %, respectively. Moreover, the concentrations of propane, ethane and ethylene increase as WHSV increased. As the propane decomposition is favoured at lower space velocities, the distribution of products obtained at 700 ºC and the lowest spatial velocity studied (24 l g_{Cat}^{-1} h^{-1}) is shown in Figure 4a. It is observed that the main reaction products are hydrogen and methane, together with ethane and ethylene in concentrations below 0.5 %. A plausible mechanism for the catalytic decomposition of propane appears in Equation 2. This propane decomposition route explains the results obtained at low space velocities and temperatures of 600 ºC or below. Besides, hydrocarbon decomposition occurs through the formation of CH_y fragments. Under certain operating conditions, these fragments can recombine to form other reaction products, such as ethylene and ethane, as observed in the experiments carried out on the Ni-Cu/Al_2O_3 catalyst at higher temperatures and WHSV (Figure 2b and Figure 4b, respectively). On the other hand, carbon formation increased as the WHSV increased reaching a CFR value of 57 g_C g_{Cat}^{-1} h^{-1} for 240 l g_{Cat}^{-1} h^{-1}. CFR increased despite shortened contact time and obtaining lower propane conversions and hydrogen selectivities.

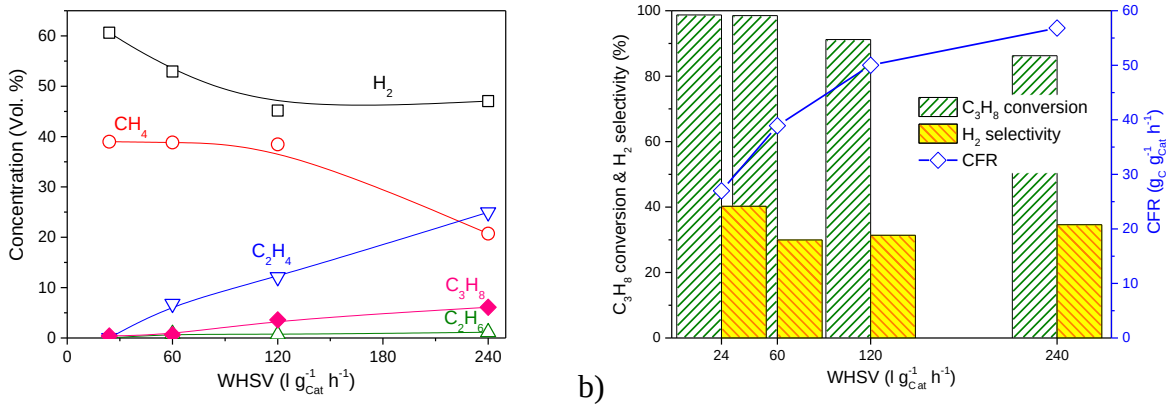

Figure 3 Influence of space velocity on the catalytic decomposition of propane: (a) initial product gas compositions; (b) propane conversions and H_2 selectivities after 10 min of reaction, and CFR values for the complete reaction. Temperature = 700 ºC.

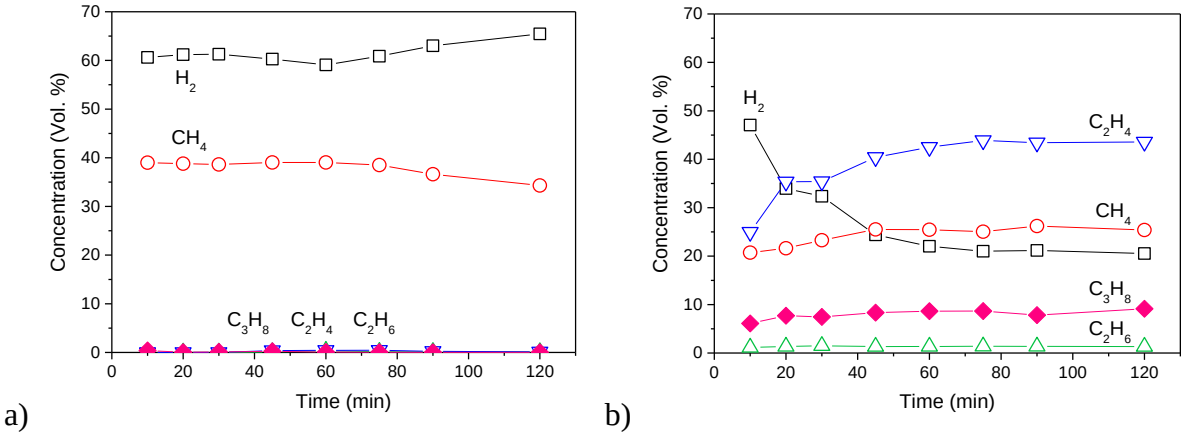

Figure 4 Distribution of products of the catalytic decomposition of propane at 700 ºC for a WHSV of a) = 24 and b) 240 l g_{Cat}^{-1} h^{-1}.

3.2 Carbon characterization

Carbon products obtained after propane decomposition were analysed by XRD to determine the crystal size (L_c) and d-spacings (d_{002}) of the graphite domains. The variation of both parameters with temperature and WHSV are shown in Figure 5a and b, respectively. d_{002} of the deposited carbon hardly varied with the operating temperature or WHSV, taking values in the range 0.339-0.347 nm. This value of d_{002} is comprised between that corresponding to perfect graphite, with d_{002} = 0.3354 nm, and that of highly disordered turbostratic carbons, in which values of 0.344 nm have been determined [31]. On the other hand, the graphite crystallite size increased with temperature showing L_c values in the range of 3.7 to 5.1 nm. The structural values obtained for CNF obtained by catalytic decomposition of propane are similar to those obtained for ethane or methane [27, 28]; however, there are trends in both parameters considering the hydrocarbon used. The higher the C/H ratio in the starting hydrocarbon, d_{002} is slightly higher and L_c is smaller in the formed CNF regardless of the operating temperature (in the range 550-750 ºC). In the case of WHSV, it substantially influenced the crystalline arrangement of the deposited carbon, as shown in Figure 5b. L_c decreased around 2 nm with an

increase in WHSV. In general terms, it can be concluded that the deposited carbon, although of a turbostratic nature, is more ordered by increasing the operating temperature and decreasing the space velocity. Likewise, carbon obtained is less ordered than that obtained in the decomposition of methane or ethane [27, 28].

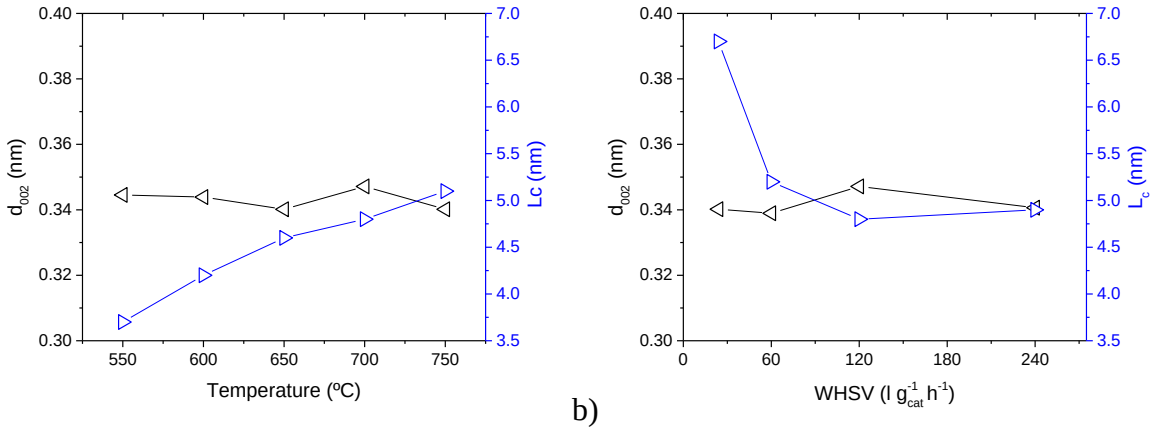

Figure 5 Evolution of structural parameters (d_{002} and L_c) of carbon nanofibers deposited on the Ni-Cu/Al_2O_3 catalyst after the decomposition of propane at a) different temperatures and b) WHSV.

Table 1 shows the textural parameters of CNF obtained by N_2 physisorption at 77 K as a function of temperature and WHSV. The BET specific surface area (S_{BET}) decreased with operating temperature. Lower temperatures resulted in CNF showing graphite crystals with smaller sizes (L_c; Figure 5a) and more open angles with the growth axis. In the case of the WHSV, a maximum for 60 l g_{Cat}^{-1} h^{-1} is observed and then a decrease for higher WHSV. In this case, the differences could be motivated by the different reaction times used (longer reaction times would result in higher carbon formations). Also, it is observed that this has the same effect on the area associated with micropores (S_{mic}). S_{BET} obtained in the propane decomposition are larger than those obtained for the decomposition of ethane and methane in previous works [27, 28]. This is due to the higher CFR obtained as the carbon product presents a higher S_{BET} than

the starting catalyst. Comparing the S_{BET} measured for carbonaceous products obtained by catalytic decomposition at 550 ºC, the following trend is observed: propane (192 $m^2\ g^{-1}$) > ethane (167 $m^2\ g^{-1}$) > methane (135 $m^2\ g^{-1}$). Although 550 ºC was the temperature reaching the highest S_{BET} values in the cases of propane and ethane, 600 ºC was the one in the case of methane. However, the S_{BET} of the carbon products obtained at 600 ºC still followed the previous trend: propane (178 $m^2\ g^{-1}$) > ethane (158 $m^2\ g^{-1}$) > methane (146 $m^2\ g^{-1}$). On the other hand, V_t follows similar trends to those observed for S_{BET}. Additionally, V_t is higher in the carbon obtained using propane than those obtained using ethane o methane.

Table 1 Textural properties of CNF (including growth catalyst) obtained by N_2 physisorption at 77 K.

	Conditions	S_{BET} ($m^2\ g^{-1}$)	S_{mic} ($m^2\ g^{-1}$)	V_t ($cm^3\ g^{-1}$)
Temperature (ºC) @WHSV = 120 l $g_{Cat}^{-1}\ h^{-1}$	550	192	37	0.448
	600	178	36	0.347
	650	164	23	0.362
	700	140	19	0.380
	750	101	3	0.234
WHSV (l $g_{Cat}^{-1}\ h^{-1}$) @T: 700 ºC	24	136	15	0.309
	60	173	20	0.381
	120	140	19	0.380
	240	117	6	0.308

The morphological study of the catalysts after use has been realized by SEM and TEM. In Figure 6, representative SEM images of CNF obtained at 550 and 700 ºC are shown. Carbon is deposited in the form of carbon nanofibers of several microns in length. It is interesting to highlight the high presence of nanofibers that show bidirectional growth (see Figure 6b), a growth mode generally observed in the decomposition of hydrocarbons that use certain bimetallic catalytic systems [25, 32]. In this case, two nanofibers emerge from a single catalyst particle exhibiting well developed crystalline faces. This kind of growth was also observed in previous works using ethane as the feedstock [28]. Using methane, these structures were

observed in some works using Ni-Cu catalysts [25], but not always [27]. In any case, the particles behind this growth are usually the widest of the sample size distribution, and they tend to produce CNF with bigger diameters and more open plane angles (angle between the graphene layers and the growth axis, as seen below using TEM) [25]. After propane decomposition at 700 ºC (Figure 6c), CNF formed are shorter than those observed in the sample at 550 ºC and, in this case, bidirectional growth was not observed. The shortening of the nanofilaments has been attributed to less controlled growth due to a high CFR [24]. In this case, the CFR increased from 30 to 50 $g_C\ g_{Cat}^{-1}\ h^{-1}$ for 550 and 700 ºC, respectively (see Figure 1b). In order to discriminate the type of nanofilaments produced with this catalyst, TEM images of the carbon products were acquired as shown in Figure 7. Previously [20, 24, 25], Ni-Cu particles resulted in fishbone-type CNF in the methane decomposition reaction at these operating temperatures (550 and 700 ºC). Fishbone CNF are characterized by the arrangement of the graphene layers forming an angle to the growth axis of the nanofibers (solid and dashed lines, respectively, shown in Figures 7a and 7c). Moreover, this angle is closer (towards the appearance of a carbon nanotube) in CNF obtained at higher temperatures [33], as can be observed comparing the CNF obtained at 550 and 700 ºC (Figures 7a-b and 7c-d, respectively). In addition to the operating temperature, the stacking angle is also motivated by the shape of the Ni-Cu alloy particle during the reaction and is more open when large and blunt particles are involved, which are present in both samples as will be shown below. Finally, the structural order of the graphite domains that conform the CNF, whose parameters were determined by XRD (Figure 5), can be seen in the images of the Figures 7a and 7c, where the stacks of graphene layers spaced at 0.34 nm are clearly visible.

Regarding the diameter of the CNF obtained, Figure 8 shows histograms of diameter normal distribution measured from TEM images. Diameter distributions were very similar since the starting catalyst is the same in both cases. Interestingly, as observed for Ni-Cu catalysts in the

methane catalytic decomposition in previous works [24], a bimodal diameter distribution was observed for both samples: small carbon nanofibers with diameters in the range 6-30 nm, and dense CNF (without an internal hollow core) with wider diameters up to 100 nm and above, which are less numerous. The formation of these dense CNF has been attributed to a carbon diffusion through the catalytic particle (also called bulk diffusion) [34] and the metal-support interaction strength [35]. Ni-Cu alloy presents a higher lattice constant than Ni favoring the bulk diffusion and the improvement in the CFR as has been found for the catalytic decomposition of methane [24]. Furthermore, according to the CNF growth mechanisms proposed by Baker *et al.* [36, 37], nanofibers can be obtained through a tip-growth mechanism, which is evidenced by the presence of nanoparticles at the ends of the nanofibers (as observed by TEM) and takes place for weak metal-support interactions.

a) 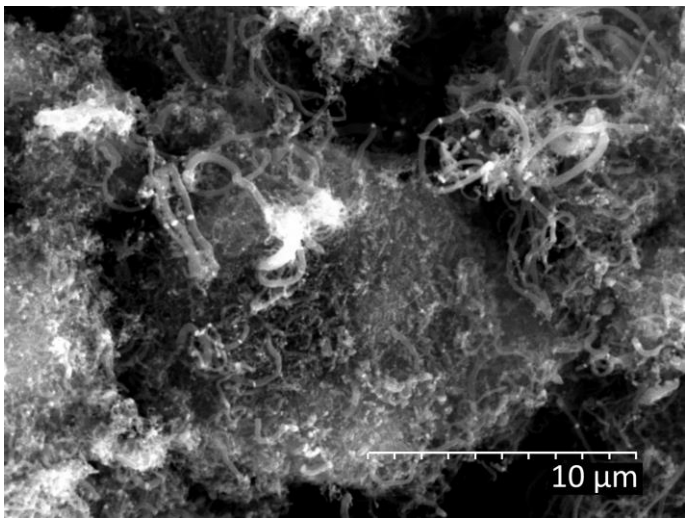

b)

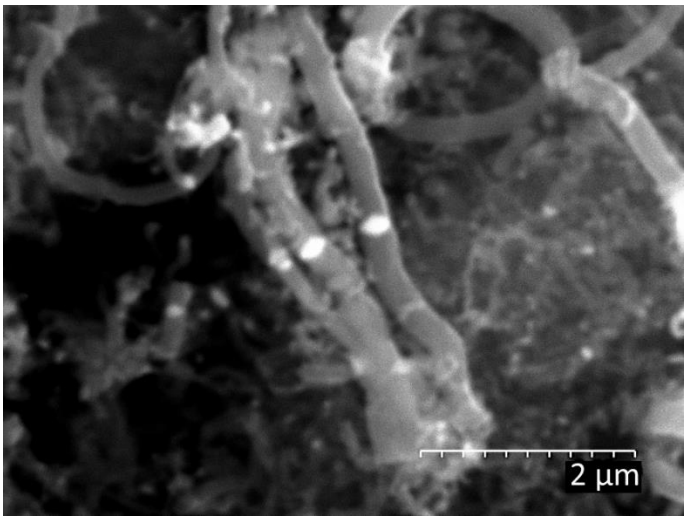

c)

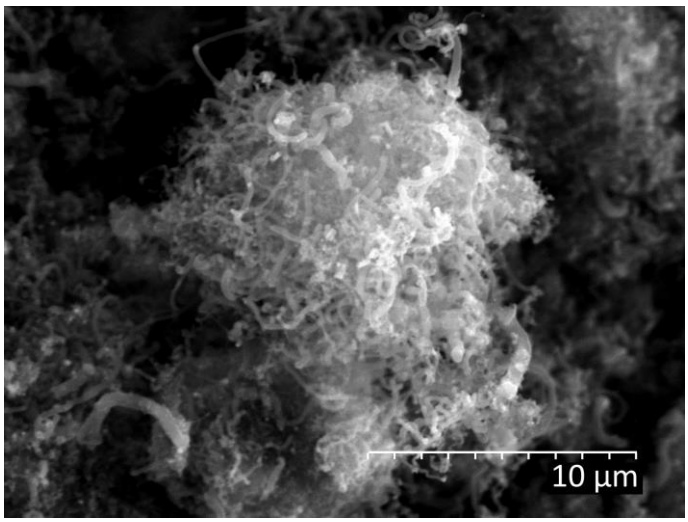

Figure 6 a) and b) SEM images of the samples obtained with the Ni-Cu/Al_2O_3 catalyst after propane decomposition at a-b) 550 ºC; and c) 700 ºC.

a)

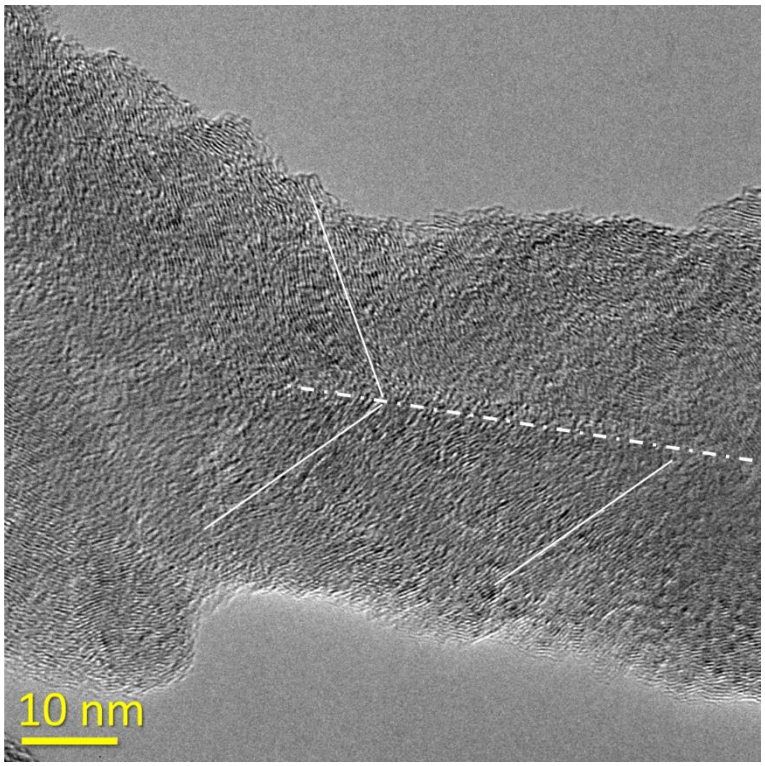

b)

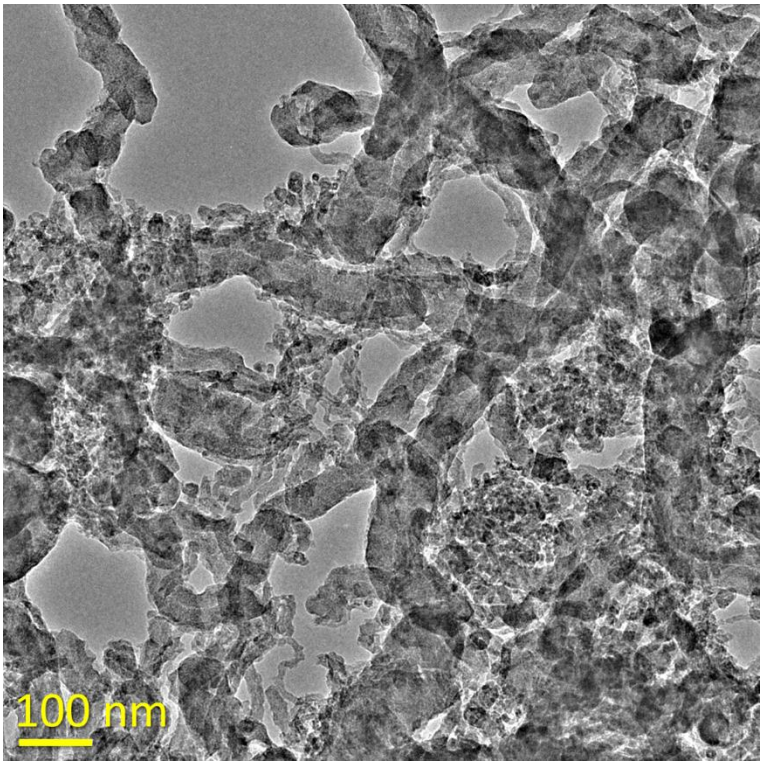

c)

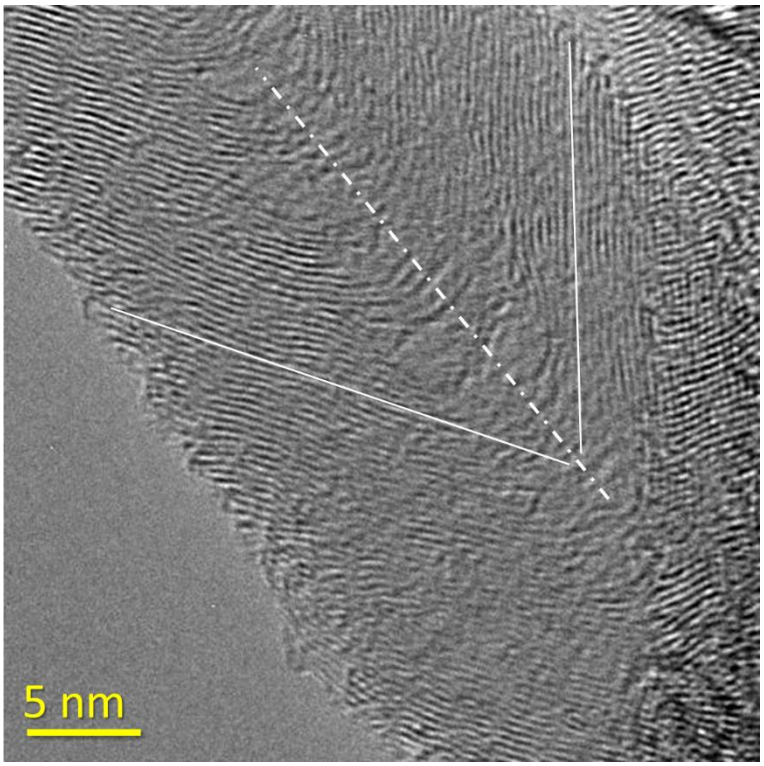

d)

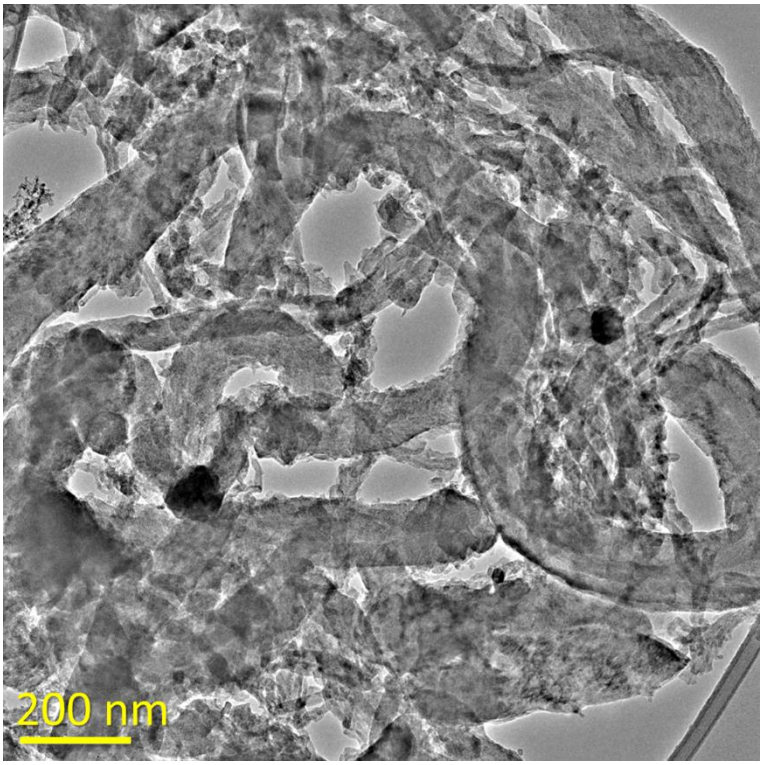

Figure 7 TEM images of CNF obtained with the Ni-Cu/Al_2O_3 catalyst after propane decomposition at a-b) 550 ºC; and c-d) 700 ºC.

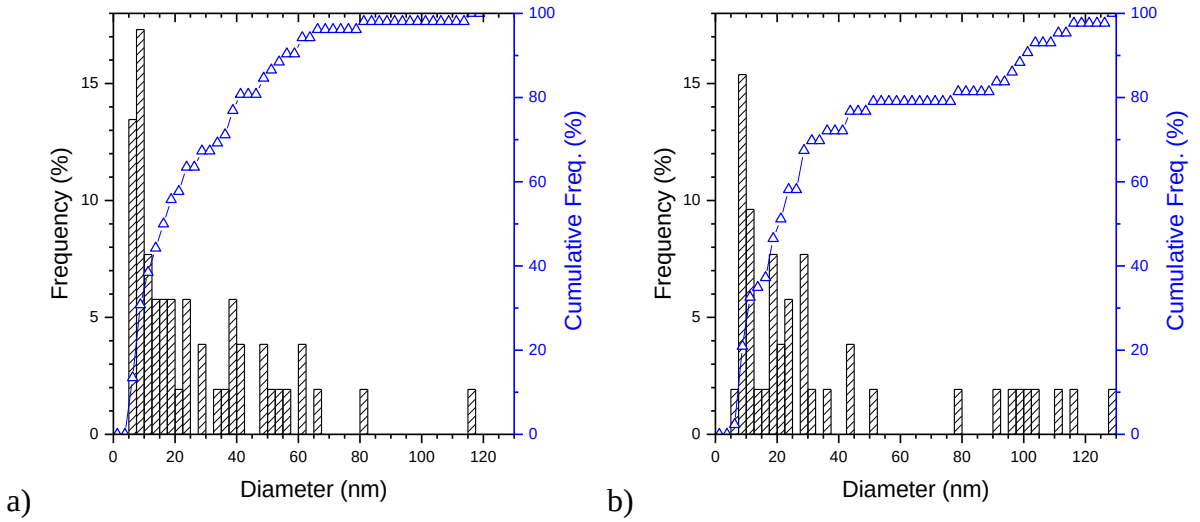

Figure 8 Histograms of diameter normal distribution of CNF obtained with the Ni-Cu/Al_2O_3 catalyst after propane decomposition at a) 550 ºC; and b) 700 ºC.

CONCLUSIONS

The catalytic thermal decomposition of propane using a Ni-Cu/Al_2O_3 catalyst to produce H_2 and high-value carbon nanofibers was evaluated in a fixed-bed quartz reactor. The reaction temperature (550-750 ºC) and the WHSV (24-120 l g_{Cat}^{-1} h^{-1}) were modified to study their effect on the propane conversion, the H_2 selectivity and the rate and quality of the carbon obtained. The main gas products detected by GC were H_2, CH_4 and C_2H_4 with small amounts of C_2H_6. Initial C_3H_8 conversion of 90 % was obtained at 700 ºC and above (using a WHSV of 120 l $g_{Cat}^{-1}h^{-1}$), while initial H_2 selectivity reached 40 % for a WHSV of 24 l $g_{Cat}^{-1}h^{-1}$ and 700 ºC of temperature. The CFR increased with temperature until reach a maximum of 50 g_C g_{Cat}^{-1} h^{-1} for 700 ºC. CNF obtained showed a wide (6-120 nm) and bimodal distribution of diameters and fishbone-type morphology. They exhibited a high graphitic order (interplanar distance: 0.339-0.347 nm, and crystal sizes around 5 nm) and good textural properties (specific surface area: 100-190 m^2 g^{-1} and total pore volume: 0.23-0.45 cm^3 g^{-1}). Ni-Cu/Al_2O_3 catalyst (78:06:16, mol. %) exhibited high activity in the decomposition of methane, ethane or propane leading to high conversions, hydrogen selectivities and high-valued carbon nanomaterials. Comparing with

ethane or methane catalytic decompositions, propane produced a higher CFR resulting in CNF with higher surface areas but lower graphitic order (higher d_{002} and lower L_c).

Acknowledgment

This work was funded by the European Regional Development Fund and the Spanish Economy and Competitiveness Ministry (MINECO) (ENE2017-83854-R).

References

[1] S. Ahmed, A. Aitani, F. Rahman, A. Al-Dawood, F. Al-Muhaish, Decomposition of hydrocarbons to hydrogen and carbon, Appl. Catal., A, 359 (2009) 1-24.

[2] H.F. Abbas, W.M.A. Wan Daud, Hydrogen production by methane decomposition: a review, Int. J. Hydrogen Energy, 35 (2010) 1160-1190.

[3] N. Shah, Y. Wang, D. Panjala, G.P. Huffman, Production of Hydrogen and Carbon Nanostructures by Non-oxidative Catalytic Dehydrogenation of Ethane and Propane, Energy Fuels, 18 (2004) 727-735.

[4] S.H. Yoon, N.-K. Park, T.J. Lee, K.J. Yoon, G.Y. Han, Hydrogen production by thermocatalytic decomposition of butane over a carbon black catalyst, Catal. Today, 146 (2009) 202-208.

[5] L.F. Albright, B.L. Crynes, W.H. Corcoran, Pyrolysis, theory and industrial practice, (1983).

[6] E.A. Solovyev, D.G. Kuvshinov, D.Y. Ermakov, G.G. Kuvshinov, Production of hydrogen and nanofibrous carbon by selective catalytic decomposition of propane, Int. J. Hydrogen Energy, 34 (2009) 1310-1323.

[7] Y. Wang, N. Shah, G.P. Huffman, Simultaneous production of hydrogen and carbon nanostructures by decomposition of propane and cyclohexane over alumina supported binary catalysts, Catal. Today, 99 (2005) 359-364.

[8] S.Y. Chin, Y.-H. Chin, M.D. Amiridis, Hydrogen production via the catalytic cracking of ethane over Ni/SiO2 catalysts, Appl. Catal. A, 300 (2006) 8-13.

[9] K. Otsuka, S. Kobayashi, S. Takenaka, Catalytic decomposition of light alkanes, alkenes and acetylene over Ni/SiO2, Appl. Catal. A, 210 (2001) 371-379.

[10] K. Otsuka, Y. Shigeta, S. Takenaka, Production of hydrogen from gasoline range alkanes with reduced CO2 emission, Int. J. Hydrogen Energy, 27 (2002) 11-18.

[11] A. Siahvashi, A.A. Adesina, Hydrogen production via propane dry reforming: Carbon deposition and reaction-deactivation study, Int. J. Hydrogen Energy, 43 (2018) 17195-17204.

[12] S.H. Yoon, G.B. Han, J.D. Lee, N.-K. Park, S.O. Ryu, T.J. Lee, K.J. Yoon, G.Y. Han, Hydorgen Production by Catalytic Decomposition of Propane Over Cabon-Based Catalyst, Korean Chemical Engineering Research, 43 (2005) 668-674.

[13] Y.H. Yun, S.C. Lee, J.T. Jang, K.J. Yoon, J.W. Bae, G.Y. Han, Thermo-catalytic decomposition of propane over carbon black in a fluidized bed for hydrogen production, Int. J. Hydrogen Energy, 39 (2014) 14800-14807.

[14] S. Neuberg, H. Pennemann, O. Wiborg, M. Wichert, R. Zapf, A. Ziogas, G. Kolb, Thermocatalytic decomposition of propane for pure hydrogen production and subsequent carbon gasification: Activity and long-term stability of Ni/Al2O3 based catalysts, Catal. Today, 242 (2015) 139-145.

[15] E. Romeo, M. Saeys, A. Monzón, A. Borgna, Carbon nanotube formation during propane decomposition on boron-modified Co/Al2O3 catalysts: A kinetic study, Int. J. Hydrogen Energy, 39 (2014) 18016-18026.

[16] S. Takenaka, K. Kawashima, H. Matsune, M. Kishida, Production of CO-free hydrogen through the decomposition of LPG and kerosene over Ni-based catalysts, Appl. Catal. A, 321 (2007) 165-174.

[17] A. Siahvashi, D. Chesterfield, A.A. Adesina, Nonoxidative and Oxidative Propane Dehydrogenation over Bimetallic Mo–Ni/Al2O3 Catalyst, Ind. Eng. Chem. Res., 52 (2013) 4017-4026.

[18] S.T. Hussain, S. Gul, M. Mazhar, F. Larachi, Synthesis of high purity carbon nano fibers and hydrogen from propane decomposition, BULLETIN-KOREAN CHEMICAL SOCIETY, 29 (2008) 389.

[19] R.K. Sahoo, H. Mamgain, C. Jacob, Influence of hydrogen on chemical vapour synthesis of different carbon nanostructures using propane as precursor and nickel as catalyst, Bull. Mater. Sci., 37 (2014) 1197-1204.

[20] I. Suelves, M.J. Lázaro, R. Moliner, Y. Echegoyen, J.M. Palacios, Characterization of NiAl and NiCuAl catalysts prepared by different methods for hydrogen production by thermo catalytic decomposition of methane, Catal. Today, 116 (2006) 271-280.

[21] S. Takenaka, Formation of pure hydrogen from methane, Res. Chem. Intermed., 32 (2006) 263-278.

[22] S.K. Saraswat, K.K. Pant, Synthesis of hydrogen and carbon nanotubes over copper promoted Ni/SiO2 catalyst by thermocatalytic decomposition of methane, J. Nat. Gas Sci. Eng., 13 (2013) 52-59.

[23] Y. Shen, A.C. Lua, Synthesis of Ni and Ni–Cu supported on carbon nanotubes for hydrogen and carbon production by catalytic decomposition of methane, Appl. Catal., B, 164 (2015) 61-69.

[24] D. Torres, J.L. Pinilla, I. Suelves, Screening of Ni-Cu bimetallic catalysts for hydrogen and carbon nanofilaments production via catalytic decomposition of methane, Appl. Catal. A, 559 (2018) 10-19.

[25] D. Torres, J.L. Pinilla, I. Suelves, Co-, Cu- and Fe-Doped Ni/Al2O3 Catalysts for the Catalytic Decomposition of Methane into Hydrogen and Carbon Nanofibers, Catalysts, 8 (2018) 300.

[26] J.L. Pinilla, I. Suelves, M.J. Lázaro, R. Moliner, J.M. Palacios, Activity of NiCuAl catalyst in methane decomposition studied using a thermobalance and the structural changes in the Ni and the deposited carbon, Int. J. Hydrogen Energy, 33 (2008) 2515-2524.

[27] I. Suelves, J.L. Pinilla, M.J. Lázaro, R. Moliner, J.M. Palacios, Effects of reaction conditions on hydrogen production and carbon nanofiber properties generated by methane decomposition in a fixed bed reactor using a NiCuAl catalyst, J. Power Sources, 192 (2009) 35-42.

[28] J.L. Pinilla, M.J. Lázaro, I. Suelves, R. Moliner, Formation of hydrogen and filamentous carbon over a Ni–Cu–Al2O3 catalyst through ethane decomposition, Appl. Catal. A, 394 (2011) 220-227.

[29] Y. Echegoyen, I. Suelves, M.J. Lázaro, R. Moliner, J.M. Palacios, Hydrogen production by thermocatalytic decomposition of methane over Ni-Al and Ni-Cu-Al catalysts: Effect of calcination temperature, J. Power Sources, 169 (2007) 150-157.

[30] J. Li, L. Shi, G. Feng, Z. Shi, C. Sun, D. Kong, Selective Hydrogenation of Naphthalene over γ-Al2O3-Supported NiCu and NiZn Bimetal Catalysts, Catalysts, 10 (2020) 1215.

[31] R. Franklin, The structure of graphitic carbons, Acta Crystallogr., 4 (1951) 253-261.

[32] A. Chambers, N. Rodriguez, R. Baker, Influence of copper on the structural characteristics of carbon nanofibers produced from the cobalt-catalyzed decomposition of ethylene, J. Mater. Res., 11 (1996) 430-438.

[33] S. Takenaka, S. Kobayashi, H. Ogihara, K. Otsuka, Ni/SiO2 catalyst effective for methane decomposition into hydrogen and carbon nanofiber, J. Catal., 217 (2003) 79-87.

[34] Y.-A. Zhu, Y.-C. Dai, D. Chen, W.-K. Yuan, First-principles study of carbon diffusion in bulk nickel during the growth of fishbone-type carbon nanofibers, Carbon, 45 (2007) 21-27.

[35] Y. Li, D. Li, G. Wang, Methane decomposition to COx-free hydrogen and nano-carbon material on group 8-10 base metal catalysts: a review, Catal. Today, 162 (2011) 1-48.

[36] R.T.K. Baker, M.A. Barber, P.S. Harris, F.S. Feates, R.J. Waite, Nucleation and growth of carbon deposits from the nickel catalyzed decomposition of acetylene, J. Catal., 26 (1972) 51-62.

[37] R.T.K. Baker, R.J. Waite, Formation of carbonaceous deposits from the platinum-iron catalyzed decomposition of acetylene, J. Catal., 37 (1975) 101-105.